nature biomedical engineering

SUPPLEMENTARY INFORMATION

https://doi.org/10.1038/s41551-018-0217-y

In the format provided by the authors and unedited.

Magnetic resonance multitasking for motion-resolved quantitative cardiovascular imaging

Anthony G. Christodoulou[1,2], Jaime L. Shaw[1,3], Christopher Nguyen[1,5], Qi Yang[1,4], Yibin Xie[1], Nan Wang[1,3] and Debiao Li[1,3]*

[1]Biomedical Imaging Research Institute, Cedars-Sinai Medical Center, Los Angeles, CA, USA. [2]Smidt Heart Institute, Cedars-Sinai Medical Center, Los Angeles, CA, USA. [3]Department of Bioengineering, University of California, Los Angeles, Los Angeles, CA, USA. [4]Department of Radiology, Xuanwu Hospital, Beijing, China. [5]Present address: Cardiovascular Research Center, Massachusetts General Hospital, Harvard Medical School, Charlestown, MA, USA. *e-mail: Debiao.Li@cshs.org

Supplementary Information

- **Supplementary Movie 1:** Video of a multitasking image with three time dimensions: inversion time, cardiac phase, and respiratory phase. The sliders control travel through each individual time dimension, allowing any contrast/cardiac-phase/respiratory-phase combination to be viewed.

- **Supplementary Figures 1–5**

- **Supplementary Note:** Effects of dictionary-based subspace training on T_1 fitting
    - **Supplementary Figures 6–7**
    - **Supplementary Tables 1–2**

- **Supplementary Method:** Motion identification
    - **Supplementary Figure 8**

Supplementary Figures 1–5

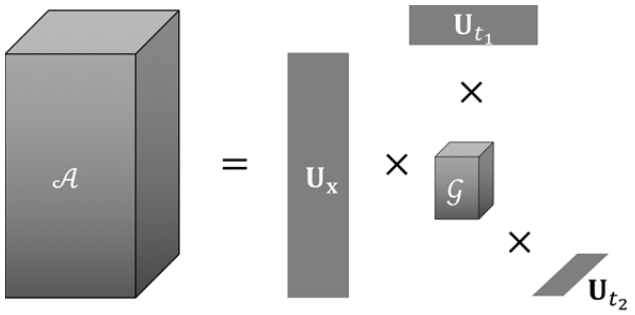

Supplementary Figure 1 | Conceptual illustration of Tucker factorization of a low-rank 3-way tensor.

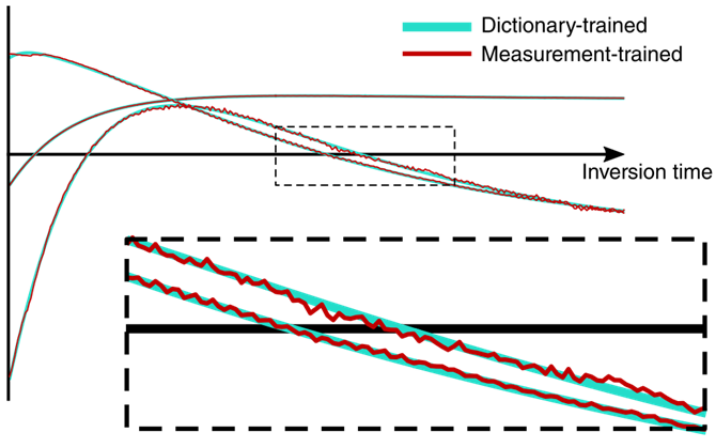

Supplementary Figure 2 | Comparison of first three T_1 relaxation basis functions learned from a dictionary of IR-FLASH signal curves to those learned from measured data.

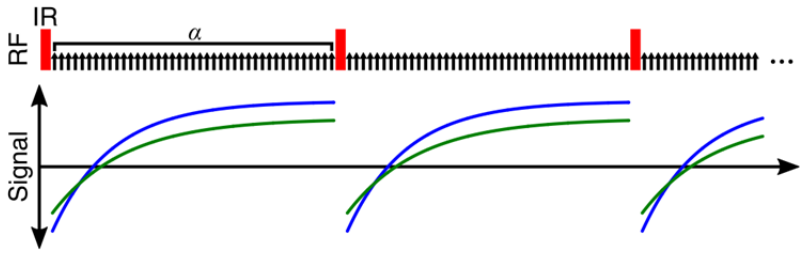

Supplementary Figure 3 | Diagram of continuous-acquisition IR-FLASH acquisition. Illustrative signal curves are shown for two tissues with different T_1 values.

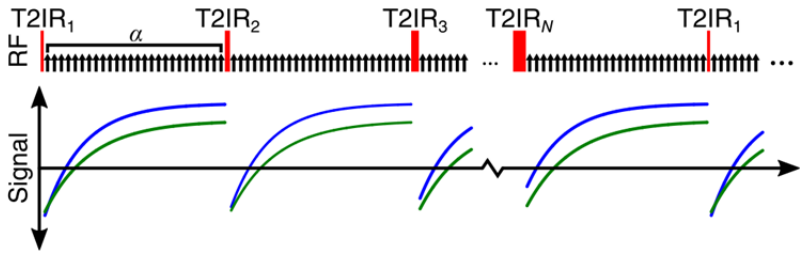

Supplementary Figure 4 | Diagram of continuous-acquisition T2IR-FLASH acquisition. Illustrative signal curves are shown for two tissues with different T_1 and T_2 values.

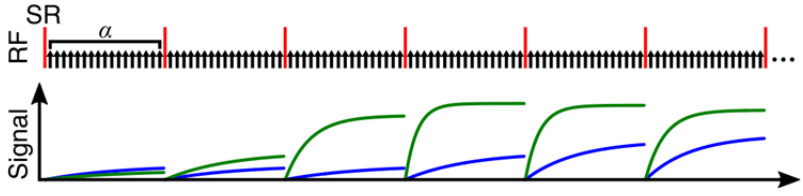

Supplementary Figure 5 | Diagram of continuous-acquisition SR-FLASH acquisition. Illustrative signal curves are shown for two tissues with different starting T_1 values and contrast agent uptakes.

Supplementary Note: Effects of dictionary-based subspace training on T_1 fitting

As described in the Methods section, it is possible to pre-determine basis functions for dynamics such as NMR relaxation, for which the space of possible signals is constrained by physics rather than subject-specific physiology. The section analyses the effects of such a pre-determined basis on T_1 fitting.

We specifically analyse the T_1 relaxation basis used to generate myocardial native T_1 mapping results, i.e., the five most significant singular vectors from the SVD of a training dictionary of IR-FLASH signal curves generated from the Bloch equations. The training dictionary contains a total of 31,815 signal curves, comprising the full Cartesian set of 101 T_1 values logarithmically spaced from 100 ms to 3 s, 15 FLASH flip angle values in half-degree increments from 0.5° to 7.5° (to account for B_1 transmit inhomogeneity), and 21 inversion pulse efficiency values linearly spaced from –1 (representing perfect inversion from a 180° preparation pulse) to –0.5 (representing imperfect inversion from a 120° preparation pulse).

The first analysis evaluates the accuracy of using only five basis functions to represent native myocardial signal curves. Sixty-one (61) IR-FLASH test curves were generated within the range of potential native myocardial T_1 values (i.e., within 800 ms to 1400 ms), on a 4x-finer grid than for the training dictionary. These curves were projected onto the subspace spanned by the pre-determined basis, and IR-FLASH signal parameters were fit from the projected curves as described in the Methods section. **Supplementary Fig. 6a** displays the normalized root-mean-square (NRMS) signal error resulting from projecting the test curves onto the pre-determined subspace; **Supplementary Fig. 6b** displays the error in T_1 resulting from nonlinear fitting of the IR-FLASH signal model to the projected curves. Five basis functions were sufficient to represent these native myocardial signal curves to within 0.37% NRMS error, with T_1 fitting accurate to within 0.24 ms absolute error.

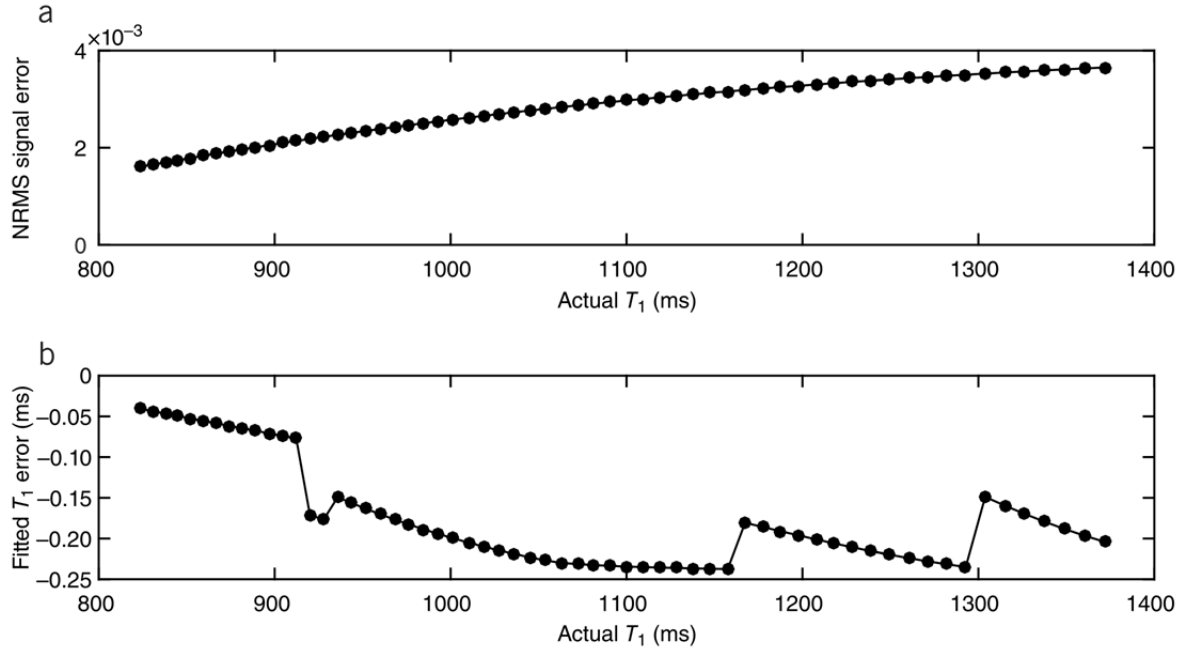

Supplementary Figure 6 | Accuracy of five dictionary-trained basis functions for representing IR-FLASH signals. (**a**) Normalized root-mean-square error from projecting IR-FLASH signal curves onto a subspace spanned by these basis functions. (**b**) Error resulting from T_1 fitting of the projected curves.

The second analysis evaluated: a) whether or not the use of the pre-determined basis biases the fitted T_1 values toward the T_1 values used in the training dictionary; and b) whether fitting is more accurate for training T_1 values than it is for T_1 values in between training elements. As before, we considered 61 T_1 values within 800 ms to 1400 ms on a 4x-finer grid than the training dictionary (so that every fourth T_1 value was used in the original training dictionary). For each testing T_1 value, a Monte Carlo simulation generated n=100 noisy signals with complex white Gaussian additive noise (SNR = 20), which were projected onto the pre-determined basis; IR-FLASH signal parameters were fit from the projected noisy curves. **Supplementary Fig. 7a** displays the bias (with 95% confidence intervals) in T_1 after fitting; the colour of each dot denotes its relative position to the nearest training T_1 value. Data were sorted into four groups based on this relative position: “closest shorter” values (test T_1 values immediately to the left of a training value), “matching” values (test T_1 values which were also used for training), “closest longer” values (test T_1 values immediately to the right of a training value), and “farthest” values (test T_1 values which bisect training values). If the

use of a training dictionary biased T_1 fitting towards T_1 values in the dictionary, we would expect to see a positive bias for the "closest shorter" group, a bias of zero for the "matching" group (and potentially the "farthest" group which bisects dictionary values), and a negative bias in the "closest longer" group. **Supplementary Figs. 7b–c** display the mean signed error and geometric mean absolute error with 95% confidence intervals for all four groups. All values were negatively biased on the order of 0.5 ms. Two-way ANOVAs (**Supplementary Tables 1–2**) were performed to test for any differences between groups and between Monte Carlo instances. These ANOVAs were performed for both signed error (i.e., bias) and absolute error; absolute error was log-transformed to better achieve normality. No significant differences were found. These analyses demonstrate that: a) use of the pre-determined basis does not bias the fitted T_1 values toward the T_1 values used in the training dictionary; and b) there is no statistically significant relationship between fitted T_1 error and distance from a training value.

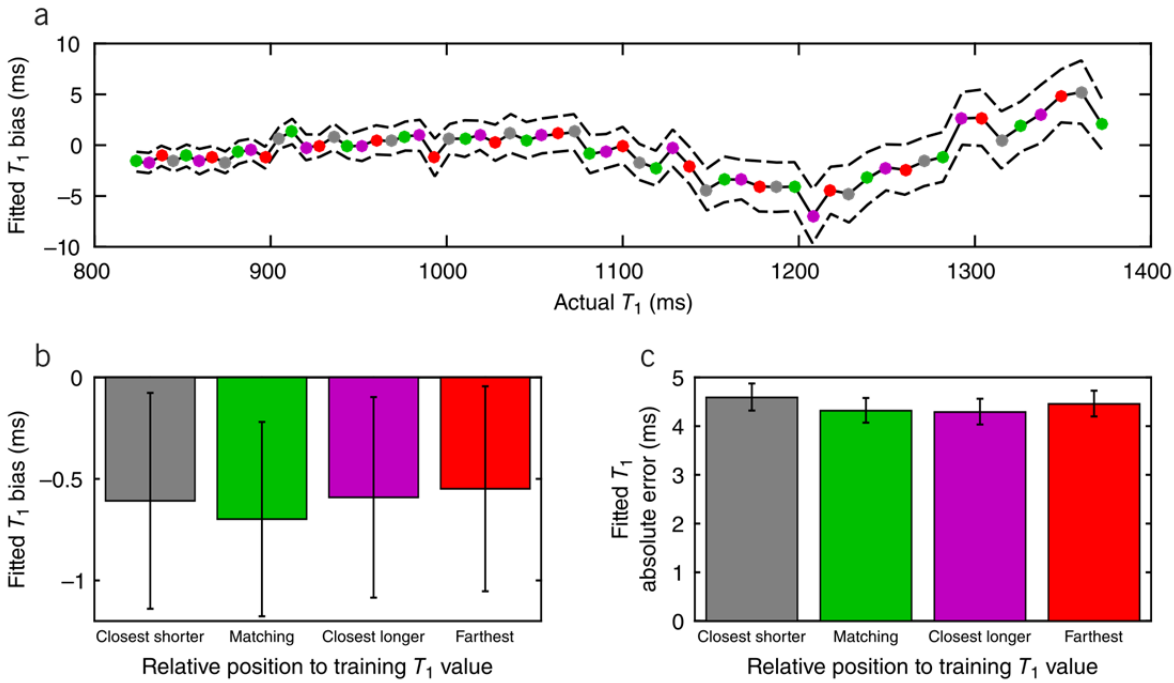

Supplementary Figure 7 | Bias and error in T_1 fitting of noisy signals (SNR = 20) projected onto five dictionary-trained basis functions. (**a**) Bias with (95% confidence interval) across the range of myocardial T_1 values, for Monte Carlo simulations of n=100 noisy signals per testing T_1 value. (**b**) Bias (with 95% confidence intervals) as a function of the testing value's relative position to the nearest training value (n=1500 noisy signals per non-matching relative position, n=1600 noisy signals per matching position). (**c**) Geometric mean absolute error (with 95% confidence intervals) as a function of the testing value's relative position to the nearest training value (n=1500 noisy signals per non-matching relative position, n=1600 noisy signals per matching position).

Source	Sum of Squares	Degrees of Freedom	Mean Squares	*F*	*p*
Relative position	18.5	3	6.18	0.062	0.98
Monte Carlo instance	7.24×10^3	99	73.2	0.728	0.98
Error	6.03×10^5	5,997	102		
Total	6.10×10^5	6,099			

Supplementary Table 1 | Two-way ANOVA table indicating no relationship between signed error and relative position of the testing T_1 value to the nearest training T_1 value in n=6100 noisy signals, demonstrating that T_1 fitting is not more accurate at training values than for values in between.

Source	Sum of Squares	Degrees of Freedom	Mean Squares	*F*	*p*
Relative position	4.40	3	1.47	1.023	0.38
Monte Carlo instance	111	99	1.12	0.784	0.94
Error	8.60×10^5	5,997	1.43		
Total	8.72×10^5	6,099			

Supplementary Table 2 | Two-way ANOVA table indicating no statistically significant relationship between absolute error and relative position of the testing T_1 value to the nearest training T_1 value in n=6100 noisy signals, demonstrating that T_1 fitting does not produce less error at training values than for values in between.

Supplementary Method: Motion identification

Construction of the multidimensional tensors for MR multitasking requires knowledge of the respiratory position and cardiac phase at every time point. There are various potential strategies for doing so using the information collected during the scan. For example, the data collected using the previously described strategy can be preliminarily reconstructed as real-time images (e.g., using explicit-subspace low-rank matrix imaging with only one time dimension representing elapsed time[1]), allowing image-based cardiac and respiratory phase identification. Alternatively, the subspace training data can be treated as self-gating lines[2] for respiratory/cardiac binning.

In this work, we chose to use an unsupervised machine learning approach to identify motion states, employing a modified *k*-means clustering algorithm incorporating a low-rank NMR relaxation model to address the variable contrast weighting of the self-gating lines. Respiratory identification was performed first, by clustering the self-gating signal $d_{\mathrm{tr}}(\mathbf{k}, t)$ into *R* respiratory bins considering the objective:

$$\arg \min_{\mathbf{r},\{\mu_r(\mathbf{k},\tau)\}_{r=1}^{R}} \sum_{i,j} \left| d_{\mathrm{tr}}(\mathbf{k}_i, t_j) - \mu_{r_j}(\mathbf{k}_i, \tau_j) \right|^2,$$

where $\mu_r(\mathbf{k}, \tau)$ is the centroid of the *r*th respiratory bin for contrast timing parameter τ (in this case, inversion/saturation time), where r_j designates the respiratory bin at the *j*th time point t_j, and where τ_j designates the contrast timing parameter at t_j. The contrast timing parameters in the vector $\boldsymbol{\tau}$ are known beforehand from the pulse sequence program, but the respiratory timing vector $\mathbf{r}$ (containing the bin assignment at each time point) and the centroids $\{\mu_r(\mathbf{k}, \tau)\}_{r=1}^{R}$ must both be determined during clustering.

As described in the Methods section, an NMR relaxation factor matrix $\mathbf{U}_{\mathrm{t}_N}$ can be pre-computed. This allows the construction of a constraint on the centroids: $\mu_r(\mathbf{k}, \tau) \in \Psi$, where the subspace Ψ is spanned by the columns of $\mathbf{U}_{\mathrm{t}_N}$. Using this low-rank centroid model, we implemented a modified *k*-means algorithm, iterating over the following steps:

1. Update the centroids: $\{\hat{\mu}_r(\mathbf{k}, \tau)\}_{r=1}^{R} = \arg\min_{\{\mu_r(\mathbf{k},\tau)\}_{r=1}^{R}} \sum_{i,j} \left| d_{\mathrm{tr}}(\mathbf{k}_i, t_j) - \mu_{\hat{r}_j}(\mathbf{k}_i, \tau_j) \right|^2$
2. Update the respiratory bin assignments: $\hat{\mathbf{r}} = \arg\min_{\mathbf{r}} \sum_{i,j} \left| d_{\mathrm{tr}}(\mathbf{k}_i, t_j) - \hat{\mu}_{r_j}(\mathbf{k}_i, \tau_j) \right|^2$
3. Low-pass filter $\hat{\mathbf{r}}$ below the cardiac fundamental frequency

For step 3, the low-pass filter cutoff was selected as 50 cycles per minute to filter out the effects of cardiac motion. This algorithm was implemented with 10 different randomly generated initial guesses of $\hat{\mathbf{r}}$; the solution with the smallest objective was selected. **Supplementary Fig. 8** illustrates one iteration of this algorithm.

Cardiac identification was then performed by a similar process, clustering the self-gating signal into *C* cardiac bins considering the objective:

$$\arg \min_{\mathbf{c},\{\mu_{r,c}(\mathbf{k},\tau)\}_{r=1,c=1}^{R,C}} \sum_{i,j} \left| d_{\mathrm{tr}}(\mathbf{k}_i, t_j) - \mu_{r_j,c_j}(\mathbf{k}_i, \tau_j) \right|^2,$$

where $\mu_{r,c}(\mathbf{k}, \tau)$ is the centroid of the *r*th respiratory bin and *c*th cardiac bin for any given τ, and where c_j designates the cardiac bin at the *j*th time point t_j. Our modified *k*-means algorithm looped through the following steps:

1. Update the centroids: $\left\{\hat{\mu}_{r,c}(\mathbf{k}, \tau)\right\}_{r=1,c=1}^{R,C} = \arg\min_{\{\mu_{r,c}(\mathbf{k},\tau)\}_{r=1,c=1}^{R,C}} \sum_{i,j} \left| d_{\mathrm{tr}}(\mathbf{k}_i, t_j) - \mu_{\hat{r}_j,\hat{c}_j}(\mathbf{k}_i, \tau_j) \right|^2$
2. Update the cardiac bin assignments: $\hat{\mathbf{c}} = \arg\min_{\mathbf{c}} \sum_{i,j} \left| d_{\mathrm{tr}}(\mathbf{k}_i, t_j) - \hat{\mu}_{\hat{r}_j,c_j}(\mathbf{k}_i, \tau_j) \right|^2$
3. Band-pass filter $\hat{\mathbf{c}}$ to the range of possible cardiac frequencies

For step 3, the passband was chosen to cover a wide range of potential heart rates from 40 bpm to 150 bpm. This algorithm was implemented with 10 different randomly generated initial guesses of $\hat{\mathbf{c}}$; the solution with the smallest objective was selected. Cardiac phases were defined from the Hilbert transform phase of the cardiac cluster vector $\hat{\mathbf{c}}$.

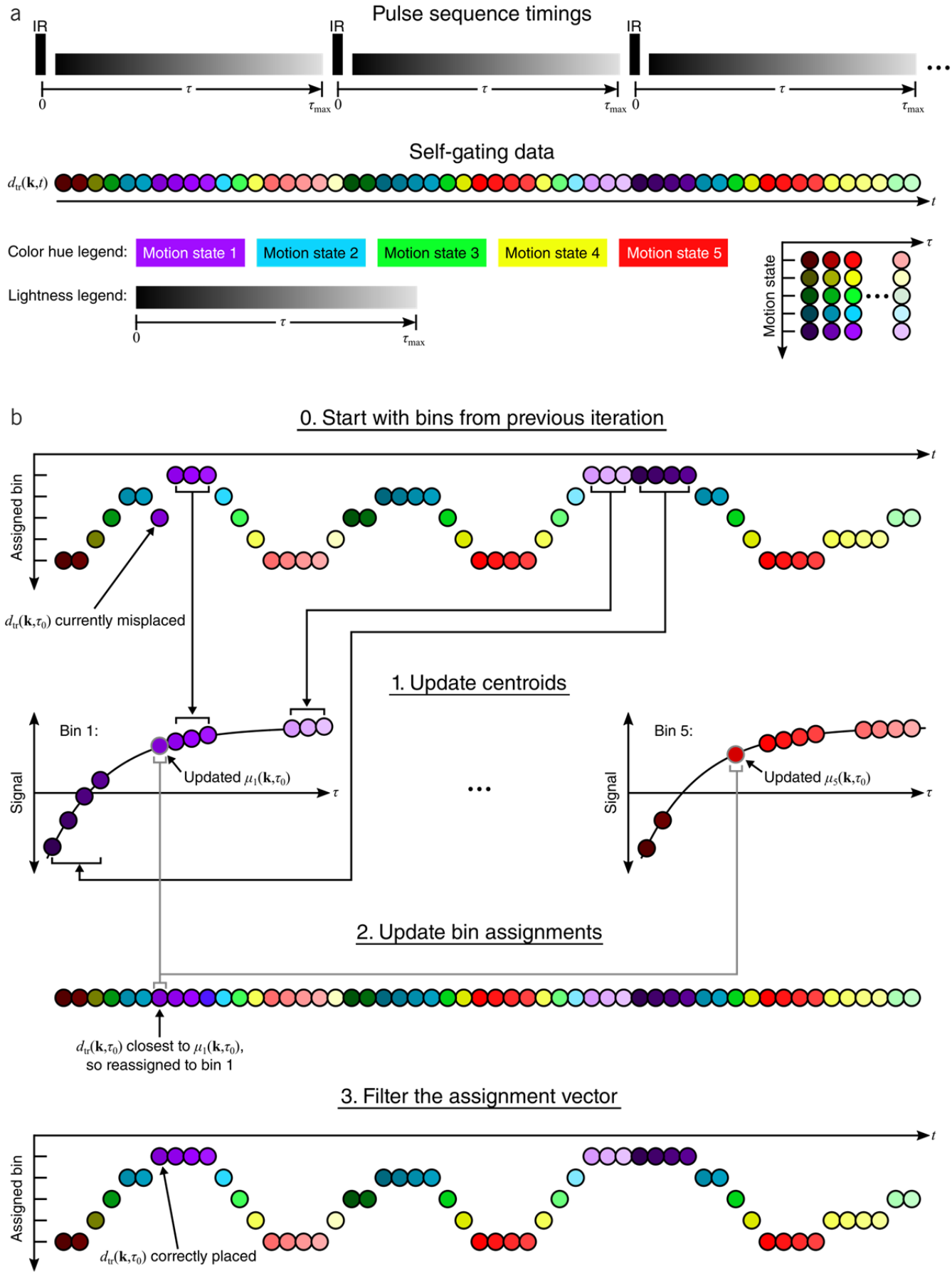

Supplementary Figure 8 | Illustration of motion clustering algorithm. (**a**) Pulse sequence timings and representation of self-gating data. Dark circles represent readouts from early inversion times; light circles represent readouts from late inversion times. The colour hue of each circle denotes the ground truth motion state at that time point. (**b**) Illustration of one iteration. Each iteration is initialized with the bin assignments from the previous iteration "step 0". In this example, the self-gating readout at time τ_0 is misclassified, being incorrectly based in the third bin when it should be in the first. In step 1, the self-gating data are temporarily assigned to motion bins according to the current guess; the T_1 recovery basis functions are fit to these data to generate centroids for each inversion time and motion state. In step 2, each self-gating readout is reclassified by comparing it to the inversion-time–matched centroid from each motion state. In this example, the self-gating readout at time τ_0 is most similar to the inversion-time–matched centroid from the first bin, so it will be reassigned to bin 1. In step 3, the vector of updated bin assignments is filtered to the range of relevant frequencies. The newly output bin assignments will be used to initialize the next iteration.

Supplementary References

1. Christodoulou, A.G. et al. High-resolution cardiovascular MRI by integrating parallel imaging with low-rank and sparse modeling. *IEEE Trans Biomed Eng* **60**, 3083-3092 (2013).
2. Larson, A.C. et al. Self-gated cardiac cine MRI. *Magn Reson Med* **51**, 93-102 (2004).